The Kinetics of Martensite Formation in Small Particles

C. L. MAGEE

The kinetics of martensite nucleation in "atomized" particles of Fe-24.2 Ni-3.6 Mn and Fe-22 Ni-0.49 C have been investigated as a function of particle size (10 to 140 μ) and reaction temperature. The dependence of particle fraction transformed on particle size indicates that martensite nucleates at surface or near-surface sites for the Fe-Ni-C powder and throughout the bulk for the Fe-Ni-Mn powder. It is shown that, in contrast to kinetic measurements on bulk samples where autocatalysis predominates, the present technique measures reaction rate due solely to the sites present initially. The measurements show that there is no detectable incubation time for nucleation and that the nucleation sites have a specific distribution of activation energies. A method for extracting the distribution from experimental measurements is given and the result is used to develop a revised equation for describing isothermal martensite formation. The isothermal kinetics of martensite formation in Fe-22 Ni-0.49 C are investigated despite the fact that such measurements are not possible in bulk samples because the alloy transforms by "bursting". It is found that the apparent activation entropy for martensite nucleation is significantly higher for this alloy than for Fe-24.2 Ni-3.6 Mn. This suggests that the dislocation-dislocation interactions at the critical nucleation step are longer-range in the Fe-Ni-C alloy than in the Fe-Ni-Mn alloy.

THE quantitative kinetic parameters describing the nucleation of martensite have been derived for the most part from analysis of isothermal transformation experiments. The characteristics of isothermal martensite formation were first documented completely by Shih, Averbach, and Cohen[1] and their results are shown in Fig. 1. In order to analyze these data, it is assumed that the heterogeneous nucleation rate,* $\dot{N}_v$ (the time derivative of the number of martensite plates per unit volume, N_v) can be written as a product of the number of nucleation sites per unit volume, n_t, and a rate of conversion of these sites. The rate is written as a product of attempts per unit time, ν, and a Boltzman factor $\exp(-Q/RT)$ where Q is the activation energy for nucleation; thus,

$$\dot{N}_v = n_t \nu \exp^{-Q/RT} \qquad [1]$$

Using this formalism, experimental data can be analyzed to yield an activation energy by estimating the number of active nucleation sites and the attempt frequency. The derived activation energies and their dependence on reaction temperature (*i.e.*, driving force) have been used as the primary quantities for comparing theory with experiment.[5,2]

A particularly difficult problem arises in assessing the number of active sites because their number is constantly changing due to the potent autocatalysis accompanying transformation (prior transformation greatly increases the nucleation rate, *i.e.*, increases the number of sites).[6] The purpose of the present paper is to report results from a kinetic technique that is capable of measuring the nucleation rate from the initial sites alone. It is thus possible to determine independently the number of active sites and hence reduce the level of assumption required in evaluating Q. Perhaps more importantly, the technique makes it possible to test several assumptions inherent to the analysis using Eq. [1]. In particular, it is possible to determine the relative effectiveness of the various transformation sites and the nature of their distribution. In addition, the technique allows one to measure nucleation rates in alloys where the bulk kinetics are so dominated by autocatalysis that meaningful isothermal measurements have not previously been obtained.

The classic small particle experiments of Cech and Turnbull[7,8] represent the starting point for the present experiments. These authors showed that the volume fraction of martensite in Fe-30 pct Ni (at given quench temperatures) decreases as the sample is subdivided into groups of smaller untransformed samples. They also demonstrated that in some of the particles no martensite formed in the most severe quench. This is one of the clearest experimental demonstrations of the

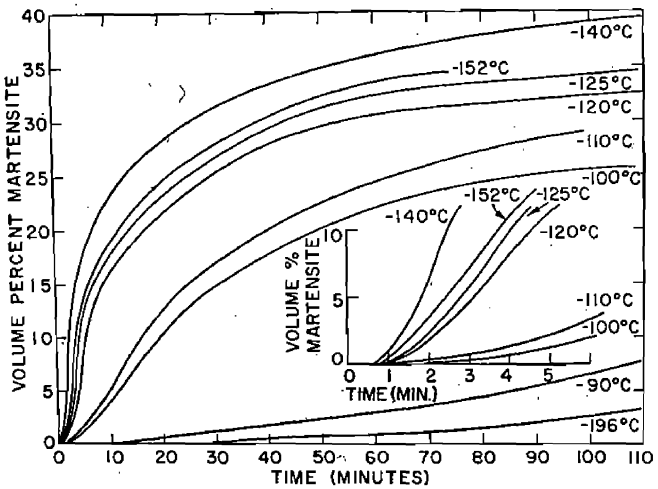

Fig. 1—Isothermal transformation results (Fe-23.2 pct Ni-3.62 pct Mn) from Shih, Averbach, and Cohen[1] showing temperature dependence and incubation time (see insert).

*The problems associated with converting the measured transformation rates to nucleation rates are covered elsewhere.[2-4]

C. L. MAGEE is with the Metallurgy Department, Scientific Research Staff, Ford Motor, Company, Dearborn, Mich.

This paper is based on an invited talk presented at a symposium on Formation of Martensite in Iron Alloys sponsored by the IMD Ferrous Metallurgy Committee and held at the Spring Meeting of the Metallurgical Society of AIME, May 1970, in Las Vegas, Nev.

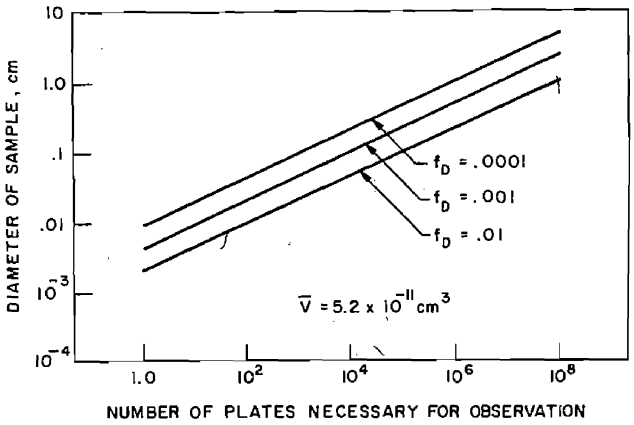

Fig. 2—Plot of the number of martensite plates in a spherical sample at detection against the sample diameter. $\overline{V}$ is the average martensite plate volume and the estimate (5.2×10^{-11} cu cm) is consistent with measurements[3,4] of this quantity. The results are shown for three different estimates of the minimum detectable transformation (f_D).

heterogeneous nature of martensite nucleation: as a given volume of austenite is divided into disconnected regions one can isolate regions which do not contain an effective nucleation site.

EXPERIMENTAL

General Considerations

In order to make measurements that actually represent the rate of transformation from a prefixed set of nucleation sites, several demands must be met. First, it is important to recognize that in the usual experiments, the "initial" transformation event corresponds to a very large number of martensite plates even using techniques with high sensitivity. However, as shown in Fig. 2, the same techniques can detect very few plates (or even the initial one) in a sample that is sufficiently small. Second, the desired measurement is the fraction of particles which transform in a group of particles where most do not transform at all. This fraction (χ'') is

$$\chi'' = N_\alpha / N_{\text{total}} \qquad [2]$$

where N_α is the number of particles containing any martensite and N_{total} is the original number of particles. In situations where χ'' is small (in order to neglect χ''^2, and so forth) and the nucleation sites randomly distributed, the ratio $\chi''/\overline{V_p}$ (where $\overline{V_p}$ is the average particle volume) is the number of nucleation events per unit volume of sample. It should be noted that one cannot simply measure the overall volume fraction of transformation, f, in a group of small particles because this does not distinguish between initial and later events and thus autocatalysis (a changing number of sites) would still dominate the measurements. The difference in measuring χ and f in a hypothetical four particle experiment is shown in Fig. 3.*

*Experiments on the solidification of small particles[8,9] can use dilatometry or other convenient measures of f because at sufficient undercooling once nucleation occurs the entire particle is solidified rapidly and so χ is essentially equal to f. However, for martensite formation, the entire particle doesn't transform.

In the present experiments, measures of χ were ob-

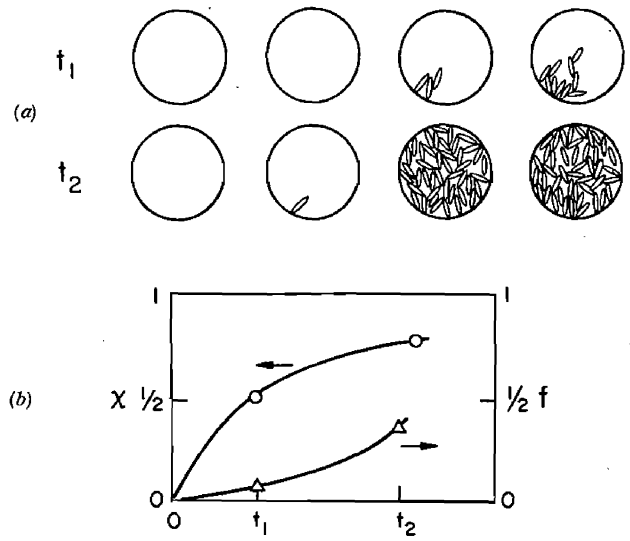

Fig. 3—(*a*) Schematic thought experiment showing progress of transformation in four particles; (*b*) particle fraction transformed (χ) and volume fraction (f) vs time for particles shown in (*a*). Note the difference in shape of the two curves.

tained by choosing alloys with paramagnetic austenites (and of course, ferromagnetic martensites) so that transformed and untransformed samples could be separated magnetically. The separated portions were weighed and

$$\chi' = \frac{\text{wt of magnetic particles}}{\text{wt of all particles}} \qquad [3]$$

was obtained. Measurement showed that the average size was the same (experimentally within ~10 pct) for transformed and untransformed samples and so $\chi'' \cong \chi'$ and we will no longer distinguish between them.

In order to obtain the parameter of interest from the measurements, a further data reduction is performed. A correction is needed for particles that transform early in the experiment and are no longer available for further transformation. The increment of transformation is $d\chi'/(1-\chi')$ and thus the total fraction of *available* particles transformed is

$$\chi = \int_0^{\chi'} \frac{d\chi'}{(1-\chi')} \qquad [4]$$

or

$$\chi = -\ln (1-\chi')$$

From a measured χ', one calculates χ and this is reported throughout the paper. We refer to this parameter as the particle fraction transformed. Note that the correction from Eq. [4] is only significant when χ is large.

Details of Experiments

Alloys were chosen so that they would 1) transform below room temperature, enabling measurements to be made easily from untransformed material, and 2) be paramagnetic as austenite to facilitate separation. One such alloy which shows completely isothermal kinetics in the bulk (Fe-24 Ni-3.65 Mn)[1,10,11] and one which transforms by bursting (Fe-22 Ni-0.49 C) were se-

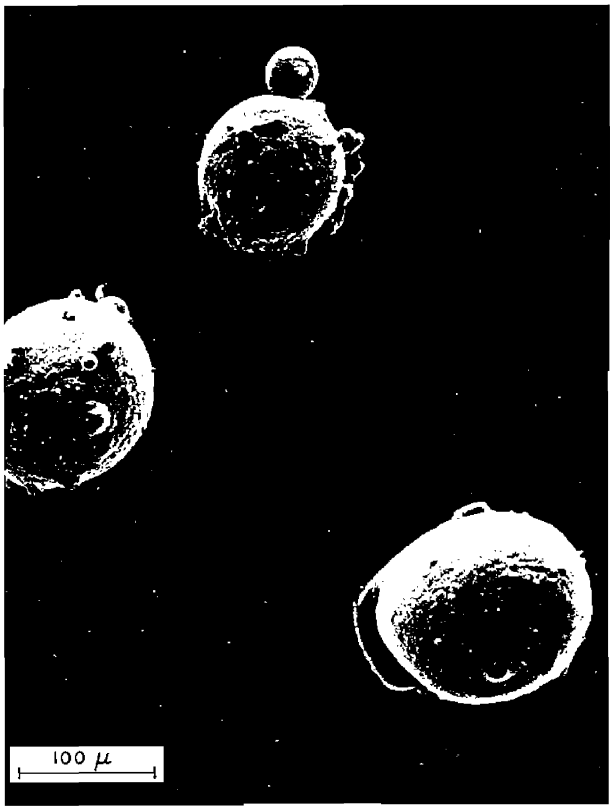

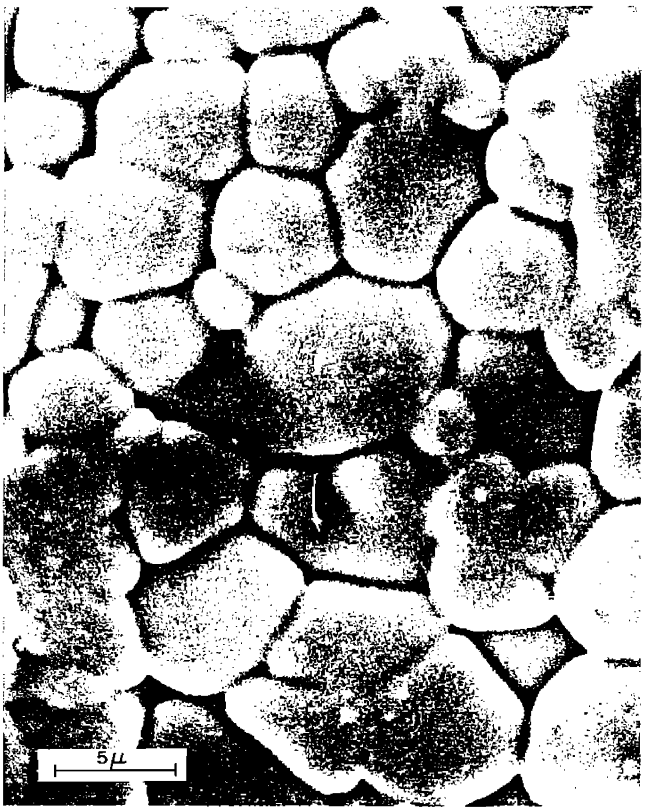

Fig. 4—Scanning electron micrographs of 135μ Fe-Ni-Mn particles at two magnifications.

Table I. Alloy Compositions and Available Particle Sizes

ıposition, ct, Bal. Fe	Size Range Mesh Number	Diameter Range, μ	Average Diameter $\bar{D}$, μ
y 1			
9Ni-3.65 Mn	+100	>150	*
1Ni-3.64 Mn	−100, +120	150 to 125	135
2Ni-3.66 Mn	−120, +170	125 to 88	98
*	−170, +325	88 to 44	70
0Ni-3.64 Mn	−325, +400	44 to 36	41
0Ni-3.68 Mn	Air	36 to 15	29
1Ni-3.69 Mn	Classifiers	15 to 5	11
y 2			
4Ni-0.484C	+100	>150	*
3Ni-0.485C	−100, +120	150 to 125	140
0Ni-0.482C	−120, +325	125 to 44	95
1Ni-0.490C	−325, +400	44 to 36	40
8Ni-0.494C	Air	36 to 15	28
0Ni-0.490C	Classifiers	15 to 5	12

Not determined.

ted. 40 lb. heats of the alloys were prepared by st melting and casting high purity materials in vac-n. The resulting ingots were then remelted and :omized'' by blowing with high purity argon at the leral Mogul Research Laboratory. All experiments ›orted here were performed on the particles re-ved after this treatment. Sizing was accomplished standard sieves and below 37 μ by air classification umns; the chemical analyses and size ranges pre-'ed are shown in Table I. The average particle di-eter determined by optical metallography using the ationship[12] $\bar{D} = \frac{3}{2}\bar{D}_p$ (where $\bar{D}_p$ is the average trav-se length of a particle) is also given in Table I.

Samples of the untransformed powders were placed in U-shaped quartz tubes and reacted in various isothermal baths (controlled to $\pm\frac{1}{2}$°C) for controlled times. The magnetic separation was then done using a series of essentially hand magnets. A magnet was used to pull particles up around the quartz container which was held in place with one arm above the other. It was necessary to use a relatively weak magnet initially so that untransformed particles were not pulled along with strongly transformed ones. Pulling them up around the U also allowed untransformed particles to fall back. Progressively stronger magnets were used until particles with sufficient magnetic response had been moved to the upper arm of the U. The two portions were then weighed with an accuracy of 10^{-4} g.

The reliability of the technique was demonstrated in several ways. 1) In extensive examination by optical microscopy no transformation was ever found in particles which we counted as ''untransformed''. In these experiments a total cross-sectional area of more than 11 sq cm was examined at 500X showing that the volume fraction transformed in these particles is surely less than 10^{-6}. It is most likely that a single martensite plate would indeed be detected by the technique but accurate calculation is difficult because the magnetic field gradient associated with the hand magnets is not known. However, the optical mocroscopy results support the idea that all transformed particles are separated. 2) When 1 g samples were remixed after separation and then separated again, the weight fraction obtained after the individual separations were identical to $\pm\frac{1}{2}$ pct which is the same accuracy obtained when the separated portions were reweighed in new containers. This experiment indicates negligible amounts of

untransformed particles were being pulled along and counted as transformed. It is important to note that this kind of reproducibility is not obtained if the strongest magnets are used in the initial stages of separation.

It is found that the reproducibility in χ for different samples reacted in the same way was not as good. For 1 and 5 g samples of 98μ particles, χ was reproducible to ±15 pct and to ±5 pct respectively. This apparently arises because of different distributions of hetereogeneities in the particles that is evident even with large numbers of particles. The results presented throughout are from 5 g samples of 98 and 135μ particles and 2 g samples of others. The number of particles is thus $\sim 10^6$ or greater in all experiments.

Characterization of Powders

The powders were studied metallographically by standard optical microscopy and scanning electron microscopy. In the case of scanning microscopy, the powders were examined directly with typical results shown in Fig. 4. It was found that many of the larger particles had sintered smaller particles adhering to them. Thus, the assumption of spherical particles is only approximate. It was also found that no difference between transformed and untransformed particles (from the same sample) could be detected by this technique indicating no gross difference in particles which contain nucleation sites. At higher magnification, Fig. 4(*b*), a grain pattern was observed on the surface having about the same size as the bulk grain size observed in specimens examined by light metallography. This suggests that the pattern was due to thermal grooving of grain boundaries.

For light microscopy, the powders were placed in coldmount while it was liquid and allowed to settle near the bottom surface. This surface was then prepared for observation by standard polishing and etching techniques. Typical results are shown in Figs. 5 and 6 for the two alloys. The optical micrographs were useful in establishing 1) that the martensite morphology (different for the two alloys) was the same in small particles as in the bulk for each alloy; 2) that the martensite in the Fe-Ni-C alloy, but not in the Fe-Ni-Mn alloy tended to be near the free surface; 3) that the grain size was $\sim 10\mu$ in both alloys and was independent of particle size; and 4) that no transformation is observed in nonmagnetic particles as noted above.

In addition to the chemical analyses reported in Table I qualitative electron probe studies were performed. In the 98μ particles, no variation in nickel or manganese was found. It should be noted that this only proves that there is no composition variation from the center to the outside of a given particle. Indeed, etching effects indicated some segregation with a spacing of about 2μ which was presumably too fine to detect with the probe beam.

RESULTS AND ANALYSIS

Particle Size Variations

In the following subsection, results from experiments with systematic variations in reaction time and

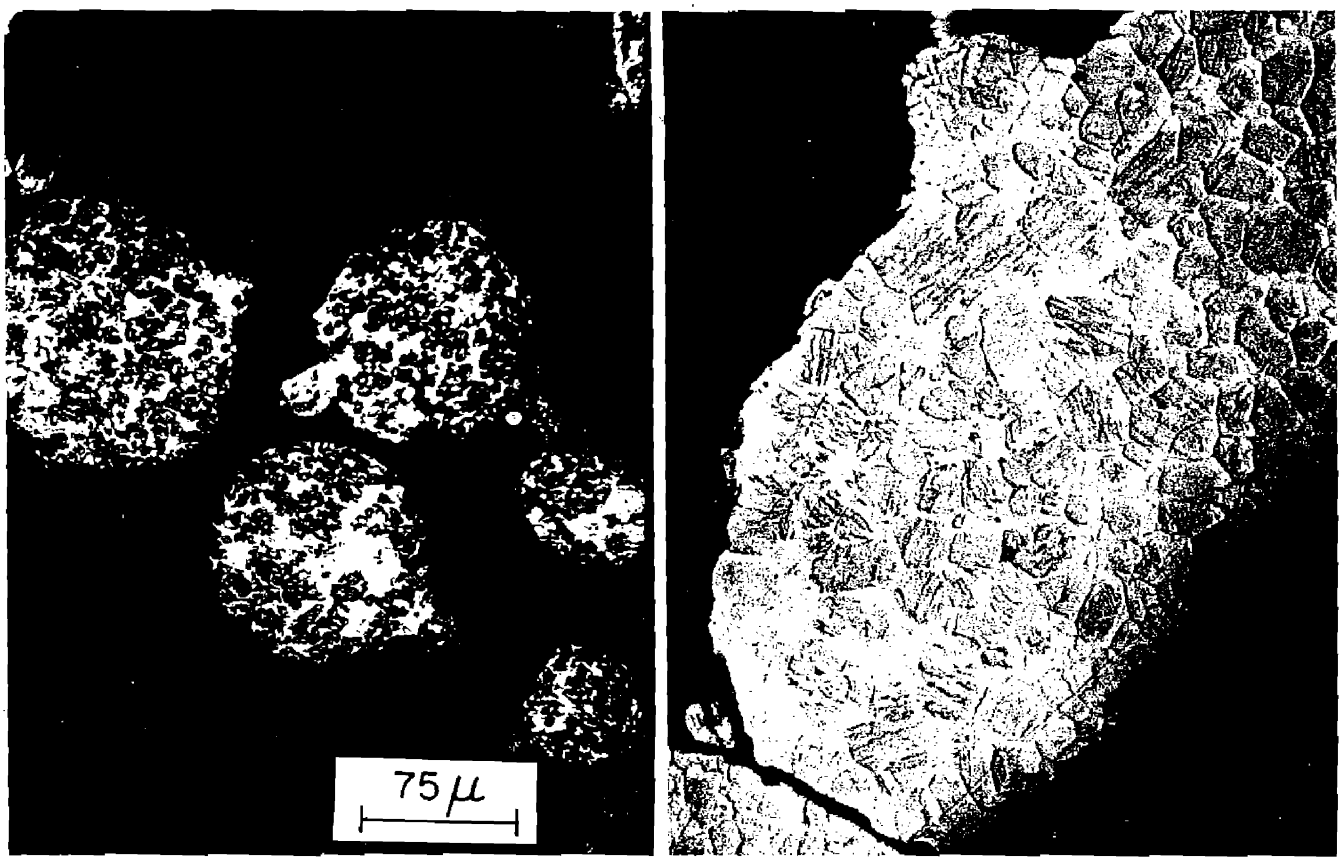

Fig. 5—Micrographs showing structure of martensite in transformed Fe-24.2 Ni-3.6 Mn particles. $\bar{D} = 98\mu$ and $> 150\mu$ on left and right respectively.

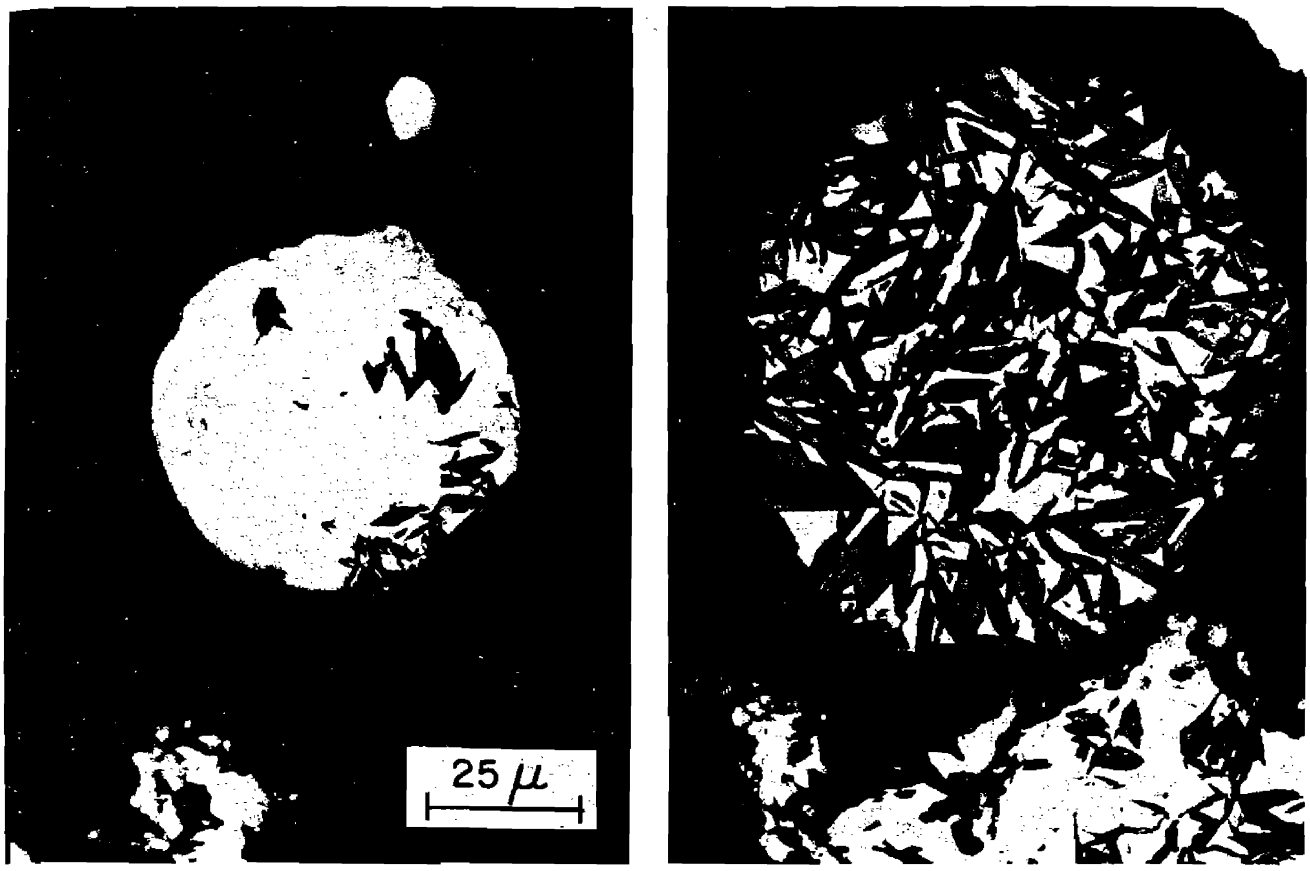

Fig. 6—Micrographs showing structure of martensite in transformed Fe-22 Ni-0.49 C particles. $\bar{D}$ = 40 and 95μ on left and right respectively.

temperature will be presented. It is useful first to consider results from instances where samples of different sized particles were reacted in identical ways. The experimental conditions and χ values are given in Table II. The results in each of these conditions can be plotted as a function of mean particle diameter ($\bar{D}$) and it is useful to plot as log χ vs log $\bar{D}$ in order to search for a power relationship. Samples with $\bar{D}$ = 98μ (95μ for Fe-Ni-C) were tested in all conditions shown; thus, all the results can be reduced to the ratio $\chi(\bar{D})/\chi(98)$ and plotted simultaneously, Fig. 7.

Lines for three different possible power relationships are also shown in Fig. 7. It is seen that the data for the Fe-Ni-Mn alloy follows a D^3 relationship. The Fe-Ni-C data falls between the D^2 and D relationships. The proportionality with D^3 found for the Fe-Ni-Mn alloy indicates that the number of effective nucleation sites per unit volume is independent of particle size.[9] The subdivision of the sample merely allows a smaller volume to count as "transformed" for each nucleation event. Thus, these results indicate that the nucleation sites are randomly distributed throughout the volume of the sample in the Fe-Ni-Mn alloy. The results for the Fe-Ni-C alloy, however, are consistent with a nucleation at surface or at near-surface sites (single spheres would then lead to a D^2 relationship but relationships between D and D^2 would be expected for spheres sintered together, Fig. 4). Indeed, the surface-nucleated reaction is not surprising and it is suspected that the absence of surface nucleation in the case of Fe-Ni-Mn may be due to a slight oxide skin. Whatever the reason, the result is fortunate in that processes more representative of bulk behavior can be studied.

Kinetic Studies

A plot of χ as a function of time at different temperatures is given in Fig. 8 for the 98μ Fe-Ni-Mn particles. Several similarities to bulk transformation curves, Fig. 1, are noted: 1) at long time, the transformation rate decreases long before all the particles are transformed, 2) the rate of transformation follows a c-curve dependence on temperature, and 3) the temperature of maximum rate, ~140°K, is the same as often found in bulk experiments.[1,10,11]

However, at short times a significant qualitative difference exists between the present results and bulk transformation behavior; that is, there is no detectable incubation time. The detailed short-time results in Fig. 9 demonstrate this. Results from both alloys, at all temperatures and for all particle sizes where meaningful measurements were made confirm this behavior.

Test for Singly Activated Process

Further kinetic information can be gained from detailed analysis of the behavior at long times. Indeed, it is thus possible to examine the assumption that all nucleation events occur with a fixed activation energy

Table II. Influence of Particle Size on Particle Fraction Transformed

$\bar{D}, \mu$	Reaction Conditions	χ
Fe-24.2 Ni-3.65 Mn		
135	2.53×10^4 sec at 195°K	0.12
98	2.53×10^4 sec at 195°K	0.067
70	2.53×10^4 sec at 195°K	0.018
41	2.53×10^4 sec at 195°K	0.002
135	1.75×10^5 sec at 215°K	0.16
98	1.75×10^5 sec at 215°K	0.066
70	1.75×10^5 sec at 215°K	0.025
135	3.6×10^4 sec at 215°K	0.11
98	3.6×10^4 sec at 215°K	0.030
70	3.6×10^4 sec at 215°K	0.016
98	5.8×10^4 sec at 163°K	0.172
70	5.8×10^4 sec at 163°K	0.06
41	5.8×10^4 sec at 163°K	0.011
29	5.8×10^4 sec at 163°K	0.010
98	3.5×10^5 sec at 163°K	0.36
70	3.5×10^5 sec at 163°K	0.15
41	3.5×10^5 sec at 163°K	0.021
29	3.5×10^5 sec at 163°K	0.017
98	8.8×10^4 sec at 133°K	0.242
41	8.8×10^4 sec at 133°K	0.012
29	8.8×10^4 sec at 133°K	0.008
		0.002
Fe-22 Ni-0.49 C		
140	9×10^4 sec at 223°K	0.073
95	9×10^4 sec at 223°K	0.040
40	9×10^4 sec at 223°K	0.012
140	9×10^5 sec at 223°K	0.41
95	9×10^5 sec at 223°K	0.24
40	9×10^5 sec at 223°K	0.075
28	9×10^5 sec at 223°K	0.061
12	9×10^5 sec at 223°K	0.016
95	2.9×10^3 sec at 195°K	0.68
40	2.9×10^3 sec at 195°K	0.145
12	2.9×10^3 sec at 195°K	0.027

(and attempt frequency). Under this assumption, the nucleation rate is merely a function of the number of sites; recall:

$$\frac{dN_v}{dt} = n_t \nu \exp(-Q/RT) \quad [1]$$

In the usual bulk experiment the total number of sites per unit volume is[13]

$$n_t = (n_i - N_v + Pf)(1 - f) \quad [5]$$

where n_i is the number present initially, N_v the number of plates nucleated per unit volume and Pf the number of sites per unit volume introduced by transformation (autocatalysis). In the present case where each particle is eliminated after any transformation and where we have allowed for those swallowed up (Eq. [4]), the total number available is

$$n_t = (n_i - N_v') \quad [6]$$

where n_i is the number of sites (per unit volume) present initially and equals $\chi^{sat}/\bar{V}_p$ where χ^{sat} is the particle fraction transformed at infinite time (all initial sites transform). N_v' is the number of these sites which have nucleated (at any time) and equals $\chi/\bar{V}_p$. Inserting these relations and $dN_v = dN_v' = d\chi/\bar{V}_p$ in Eq. [6] and the result in Eq. [1] yields

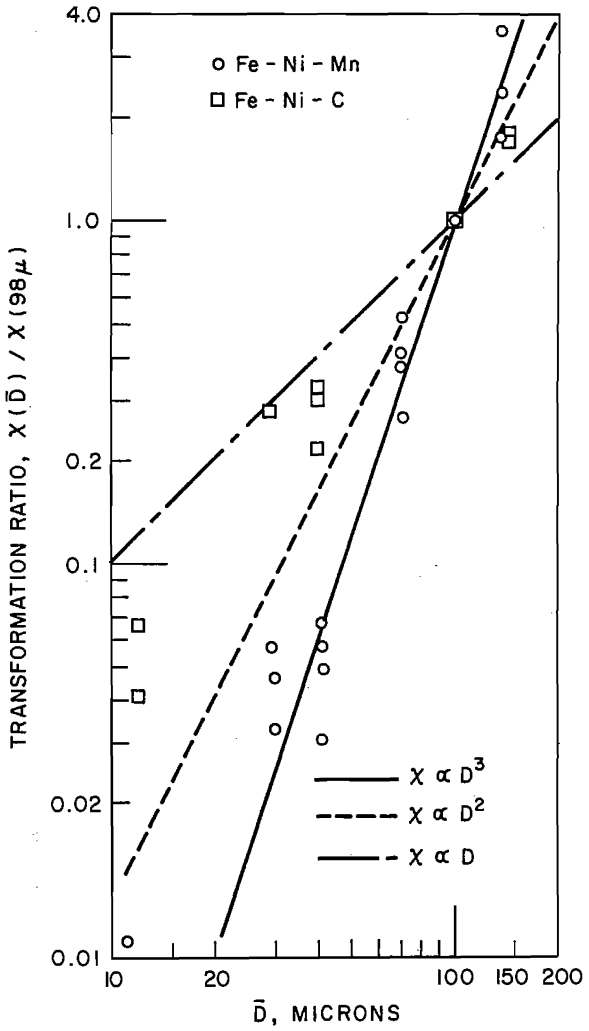

Fig. 7—Log-log plot of particle fraction transformed against average particle diameter $\bar{D}$; the particle fraction transformed is normalized to $\bar{D} = 98$ and 95μ for Fe-24.2 Ni-3.6 Mn and Fe-22 Ni-0.49 C respectively.

$$\frac{d\chi}{dt} = (\chi^{sat} - \chi)\, \nu \exp(-Q/RT) \quad [7]$$

which can be directly integrated to give

$$\ln\left(\frac{\chi^{sat} - \chi}{\chi^{sat}}\right) = -t/\tau \quad [8]$$

where

$$\tau \equiv \frac{1}{\nu} \exp(Q/RT)$$

Eq. [8] is the well-known exponential law for a singly activated process derived for the present case. If singly activated, the data when plotted as $\ln[(\chi^{sat} - \chi)/\chi^{sat}]$ vs time should yield a straight line. The problem in performing this test is that χ^{sat} could only be determined by waiting infinite time. In practice one estimates a value for χ^{sat} (*e.g.*, slightly greater than χ_{final}) in order to plot the data in the form suggested by Eq. [8]. If curvature appears, a new estimate of χ^{sat} is used. Plots of this kind for the 98μ particles reacted at 195°K are given in Fig. 10 for two values of χ^{sat}. For this data, straight lines are not obtained at any value of χ^{sat}. The critical test is that upon using lower values of χ^{sat} sure double curvature is encountered (*e.g.* at $\chi^{sat} = 0.18$ in Fig. 10). This test fails

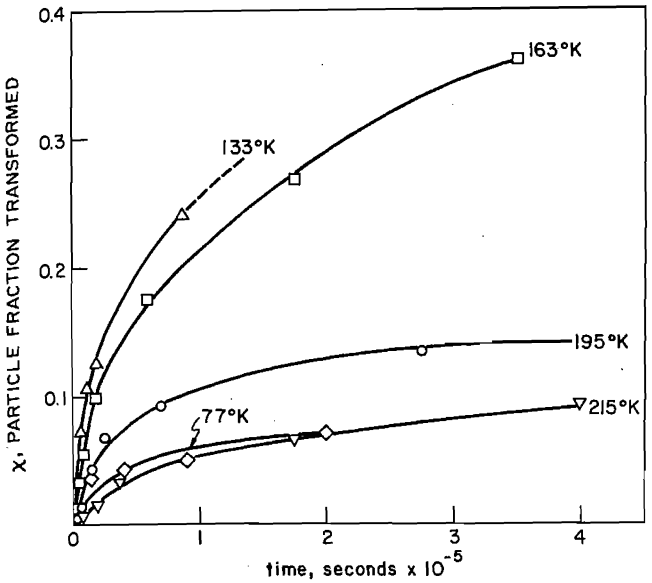

Fig. 8—Particle fraction transformed as a function of time at various temperatures for 98μ Fe-24.2 Ni-3.6 Mn particles.

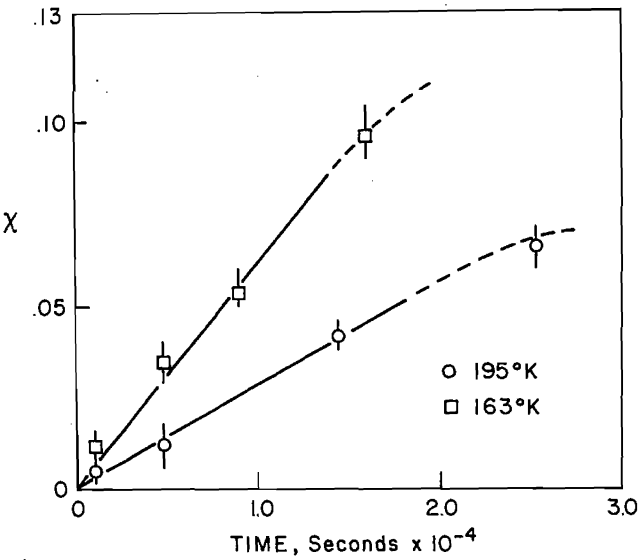

Fig. 9—Results from Fig. 8 showing details at short time.

for all situations where extensive isothermal results are available. Phenomenologically, the failure occurs because the transformation rate is greater at relatively long times than one would estimate from short times.

Before interpreting this result it is useful to discuss first two explanations that are specific to the present technique. First, there is the possibility that variations in composition cause the process to appear not singly activated. Table III shows results from several experiments where the reacted and unreacted samples are analyzed after various degrees of transformation. No difference in composition is found and the degree of reproducibility is such (<0.1 wt pct) that no appreciable smearing could arise from this source. A second possible explanation could be based on the dispersion of particle sizes present in each sample. However, if the process is singly activated for each specific particle size, then the overall average (which is measured) from the distribution would still behave in the same fashion.

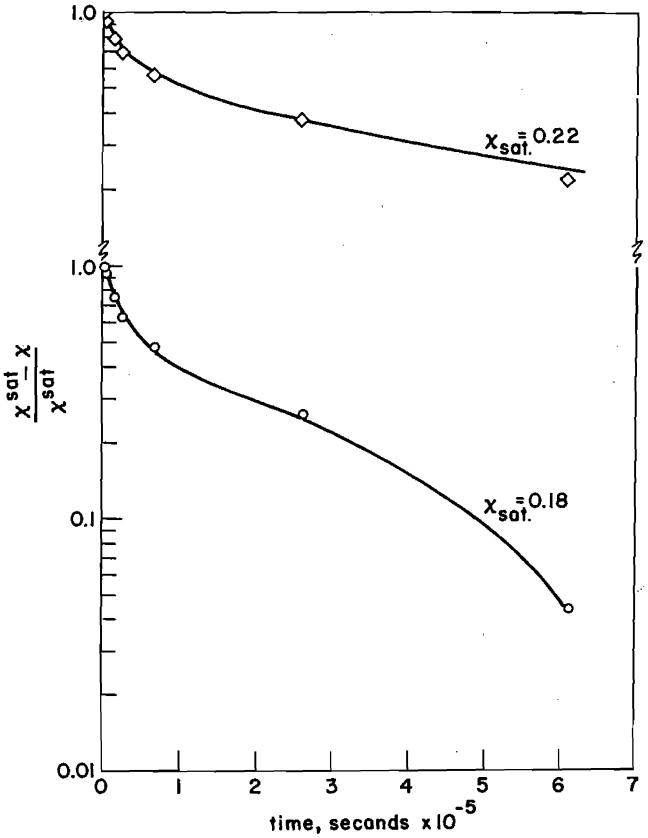

Fig. 10—Plot to test Eq. [8] shown for two estimates of the particle fraction transformed at infinite time (χ^{sat}). The results are from 98μ particles of Fe-Ni-Mn reacted at 195°K.

Table III. Chemical Analysis of Reacted Particles

Reaction Conditions	χ	Composition, Wt Pct	
		Transformed	Untransformed
98μ particles; 5.8 X 10^4 sec at 163°K	0.172	24.14Ni-3.63 Mn	24.18Ni-3.65 Mn
98μ particles; 3.5 X 10^5 sec at 163°K	0.36	24.22Ni-3.64 Mn	24.17Ni-3.65 Mn
135μ particles 1.8 X 10^5 sec at 195°K	0.39	24.20Ni-3.61 Mn	24.19Ni-3.66 Mn
140μ particles; 9 X 10^5 sec at 223°K	0.41	22.15Ni-0.485C	22.10Ni-0.48C

The relaxation time is independent of particle size so one arrives at Eq. [8] where χ and χ^{sat} are replaced by average quantities defined by

$$\bar{\chi} = \sum_i F_i \chi_i \qquad [9]$$

where F_i is the fraction of particles in the sample having particle size i and χ_i is the particle fraction transformed in particles of that size. Thus, the failure of Eq. [8] to describe the process is most reasonably interpreted as showing that martensite nucleation (from the sites present initially) is not a singly activated process.

Multiply Activated Nucleation

Analysis of multiply activated processes has received considerable attention in other problem

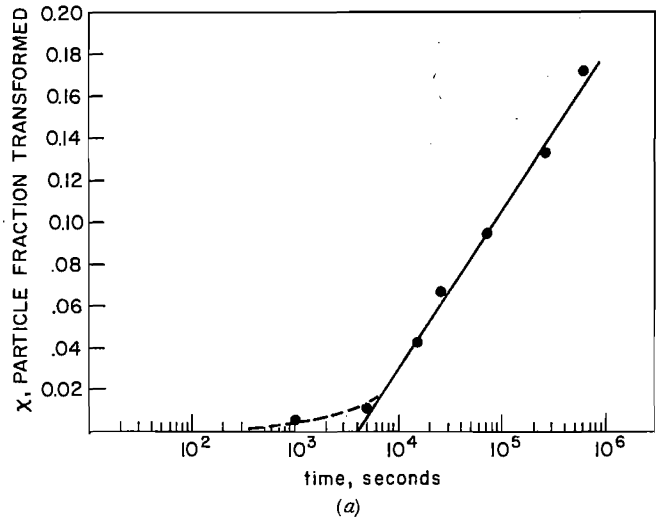

(a)

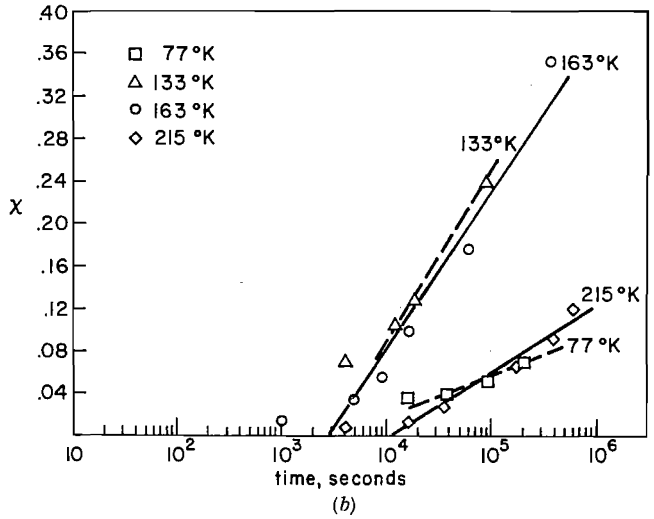

(b)

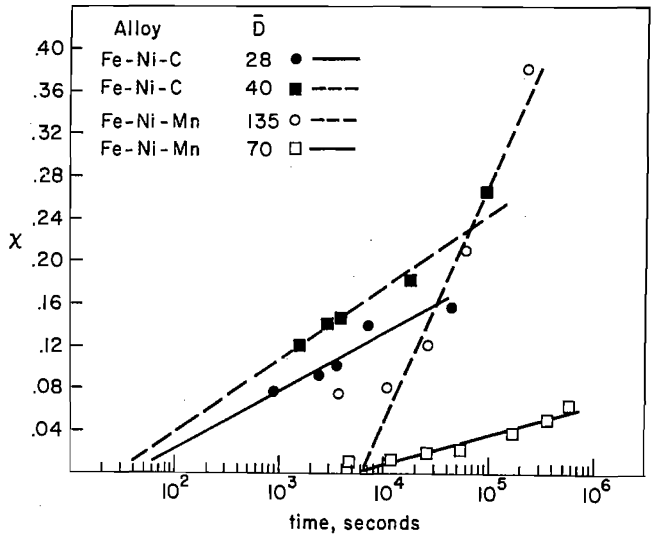

(c)

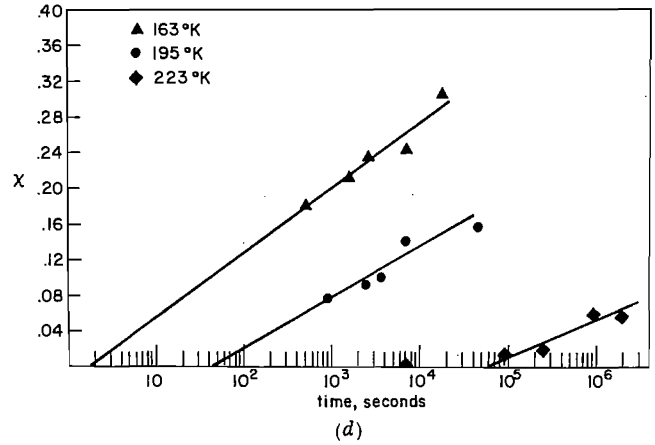

(d)

Fig. 11—Particle fraction transformed as a function of time. (*a*) Fe-24.2 Ni-3.6 Mn at 195°K, 98μ particles, (*b*) Fe-24.2 Ni-3.6 Mn; 98μ particles at various temperatures, (*c*) Fe-24.2 Ni-3.6 Mn and Fe-22 Ni-0.49 C at two particle sizes; all samples reacted at 195°K, (*d*) Fe-22 Ni-0.49 C; 28μ particles at three reaction temperatures.

areas.[14-16] The present data allow application of that formalism to martensite nucleation. Retaining the basis equation that the rate depends on the product of an attempt frequency and an exponential, the spread of τ's can be explained as being due to a distribution of ν and/or Q values. A standard approach is to hypothesize a more complicated relaxation process, *e.g.* 2 or 3 Q's, or a specific continuous distribution of Q's, and test the fit with experiment.[14,15] Without a physical basis for choosing a distribution function, this approach is not enlightening because several sufficiently complex alternatives adequately describe the data.

In the present case, a more satisfactory procedure is to analyze the data to derive a distribution. This approach has been very usefully demonstrated by Kimmel and Uhlmann[16] and by Primak[17,18] As emphasized by Kimmel and Uhlmann, it is possible to derive distributions for Q assuming ν fixed and for ν assuming fixed Q but not for simultaneous distributions of ν and Q. Further, since the experiments of necessity are performed with finite times, approximations must be employed. For the present case, the appropriate results are:[16]

$$\chi^*(\bar{Q}) \simeq 1/kT[d\chi(t)/d\ (\ln t)] \qquad [10]$$

where $\chi^*(\bar{Q})\, d_Q$ is the contribution to χ at time t from processes having activation energies between $\bar{Q}$ and $\bar{Q} + dQ$ and therefore $\chi^*(Q)$ is the distribution function for χ as a function of activation energy Q. At the same time,

$$\bar{Q} \simeq kT\ [\ln \nu t + \gamma] \qquad [11]$$

where $\gamma = 0.577$ is Euler's constant. Thus, from measurements of $d_\chi/d\ (\ln t)$ at various times and estimation of an attempt frequency, one derives the distribution as a function of activation energy. The corresponding approximate frequency distribution is obtained from[16]

$$\chi^+(\nu) \simeq 1/t\ [d\chi(t)/d(\ln t)]_{t=1/\nu} \qquad [12]$$

where $\chi^+(\nu)d\nu$ is the contribution to χ at time t from processes having attempt frequencies between ν and $\nu + d\nu$.

In Eqs. [10] and [12], the important parameter is $d\chi/d\ (\ln t)$. For this reason, a plot of χ vs $\ln t$ yields fundamental information about the distribution; much of the data from the present investigation is given in this form in Fig. 11. The results can be described by a number of curves fitting the data but the simplest consistent form is a slight curving up followed by a

straight line as shown in Fig. 11(*a*). The straight lines in Fig. 11 were arrived at through a least squares analysis (error in χ) ignoring the initial point. An important facet concerning the shape of the χ-ln t plots, Fig. 11, is that no decrease in $d\chi/d$ (ln t) at long times is seen in any of the results; thus, there is no indication that the distributions represent a broad smear about a single activation energy.*

*For a singly activated process, χ would vary sigmoidally with ln t.

The distributions (in ν and Q) derived from Fig. 11(*a*) are given in Fig. 12. The small range of Q's derived from the data is preferred over the large spread in ν, Fig. 12(*b*). Some distribution of ν might be expected but the finite probabilities at very low ν do not seem physically reasonable. Thus, somewhat arbitrarily, the distribution will be described as resulting from a range in Q only and the result is approximately a Heaviside function,[19] Fig. 12(*a*). Two parameters describe this distribution, 1) $\chi^{*\prime}(Q)$ in the constant region which is derived from the slopes of the straight lines in Fig. 11 using Eq. [10] and 2) Q_{min} which is derived from the intercept at $\chi = 0$ on Fig. 11 using Eq. [11]. Table IV summarizes these values for the various experiments. Also given in the table is $n^{*\prime}(Q)$ [$\equiv \chi^{*\prime}(Q)/\bar{V}_p$] where $\bar{V}_p$ is the average particle volume;† $n^*(Q)dQ$ is the number of sites per unit volume having activation energies between Q and $Q + dQ$. Thus, $n^{*\prime}(Q)$ and Q_{min} determine the kinetics in a bulk sample. The significance of $n^{*\prime}(Q)RT$ will be shown in the discussion section.

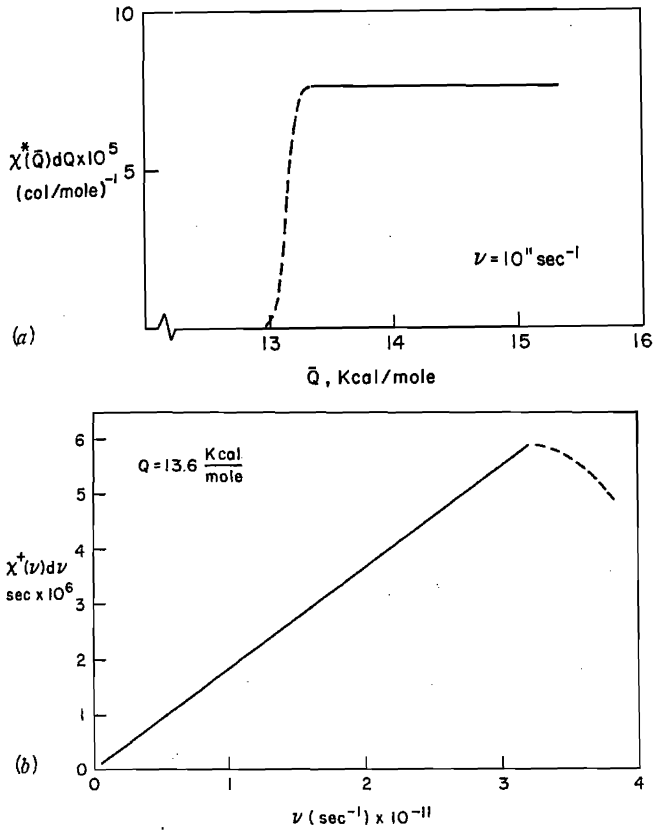

Fig. 12—Distribution functions derived from 98μ Fe-Ni-Mn particles reacted at 195°K. (*a*) Distribution with activation energy assuming fixed attempt frequency ($\nu = 10^{11}$sec^{-1}). (*b*) Distribution with attempt frequency, ν, assuming fixed activation energy, Q = 13.6 kcal per mole.

†This is calculated from $\bar{D}$, Table I, assuming spherical particles.

In Table IV it is seen that $n^{*\prime}(Q)$ is independent of particle size for Fe-Ni-Mn but not for Fe-Ni-C consistent with the results in the preceding section on particle size variations. Q_{min} is independent of particle size for both alloys and depends only on temperature. A plot of Q_{min} as a function of temperature is given in Fig. 13; the significant difference in slope for the two alloys will be discussed below.

DISCUSSION

Magnitude of Activation Energy

In the present experiments, the rate of transformation from a prefixed set of sites is measured; thus, it is not necessary to estimate the number of nucleation sites per unit volume. Hence, the kinetic parameters—the activation energy and its dependence on temperature—can be calculated with one less arbitrary parameter. It is therefore worthy of note that the magnitude of the activation energy is not seriously different and so previous uses of this kind of data (*e.g.*, to eliminate homogeneous classical nucleation)[5] are still valid. It should also be noted that we still must estimate an at-

Table IV. Distribution Parameters at Fixed Attempt Frequency (10^{11} sec^{-1})

Reaction Temperature, °K	Average Particle Diam., μ	Q_{Min}, Kcal per mole	$\chi^{*\prime}(Q)$, cal per mole^{-1}	$n^{*\prime}(Q)$, cu cm-cal per mole^{-1}	$n^{*\prime}(Q)RT$, cm^{-1}
A) Fe-24.2Ni-3.65 Mn					
195	135	13.5	26.6×10^{-5}	2.0×10^{2}	7.8×10^{4}
215	98	15.1	6.3×10^{-5}	1.2×10^{2}	5.1×10^{4}
195	98	13.3	8.3×10^{-5}	1.7×10^{2}	6.6×10^{4}
163	98	11.1	20.5×10^{-5}	4.0×10^{2}	13.0×10^{4}
133	98	9.0	26.8×10^{-5}	5.3×10^{2}	14.0×10^{4}
77	98	5.2	11.3×10^{-5}	2.2×10^{2}	3.4×10^{4}
195	70	13.3	3.3×10^{-5}	1.8×10^{2}	7×10^{4}
163	70	11.0	7.1×10^{-5}	3.9×10^{2}	12.7×10^{4}
B) Fe-22Ni-0.49C					
195	40	11.4	7.4×10^{-5}	2.2×10^{3}	0.86×10^{6}
223	28	16.6	4.1×10^{-5}	3.8×10^{3}	1.7×10^{6}
195	28	11.5	6.4×10^{-5}	5.8×10^{3}	2.2×10^{6}
163	28	8.6	9.5×10^{-5}	8.6×10^{3}	2.8×10^{6}

tempt frequency and have chosen 10^{11}sec^{-1} with discussion of this found elsewhere.[2] Since the rate depends on Q exponentially, inaccurate estimates of ν (or the number of sites) cannot easily have a major effect on the derived activation energy.

Incubation Time

The present experiments have demonstrated that no incubation time is observed for nucleation from a fixed number of nucleation sites. This observation is direct confirmation of an assumption that arises in using Eq. [1]. In particular, Raghavan and Entwisle's important technique for evaluating autocatalysis[6] is validated. In this technique, the incubation behavior is wholly attributed to autocatalysis. Thus, the estimates of the relative effectiveness of autocatalytic and initial nucleation sites obtained by numerical[6,13] or analytical procedures[2] are realistic.

Mechanistically, the lack of an incubation time indicates that no detectably slow precursor steps occur in the nucleation process. At least some of the sites are initially capable of immediately nucleating a martensite plate.

Analysis of Isothermal Kinetics From Sites Having a Distribution of Activation Energies

The fact that there is a distribution of nucleation site effectiveness has been neglected in previous isothermal analyses (Eq. [1] assumes all sites have the same Q). From the present results, a simple alternative to this procedure can be developed. For a sample with nucleation sites having a distribution of activation energies, the nucleation rate would be

$$\frac{dN_v}{dt} = \int_0^\infty \nu \exp(-Q/RT) n^*(Q) dQ \qquad [13]$$

where $n^*(Q)dQ$ is the number of nucleation sites per unit volume (χ^*/V_P) having activation energies between Q and $Q + dQ$. If we use the simplest distribution suggested by the results in Fig. 11, *i.e.*, $n^*(Q)$ constant above Q_{min} [$\equiv n^{*\prime}(Q)$] and equal to zero below Q_{min}, Eq. [13] can be integrated to give the nucleation rate at any time as

$$\frac{dN_v}{dt} = n^{*\prime}(Q)RT\ \nu \exp(-Q_{min}/RT) \qquad [14]$$

Based on the present experiments, Eq. [14] is superior to Eq. [1] for describing isothermal kinetics. The two equations are of the same form and comparison shows that

$$n_i = n^{*\prime}(Q)RT \qquad [15]$$

and that

$$Q = Q_{min} \qquad [16]$$

Thus, estimates of n_i have represented estimates of $n^{*\prime}(Q)$ and the previously calculated activation energies are the minimum energies in the distribution at the time of measurement. Hence, comparison of previous activation energies with Q_{min} is appropriate and as mentioned above shows no significant discrepancy. In contrast, however, experimental values of $n^{*\prime}(Q)RT$, Table IV, range from 3×10^4 to 2×10^5 per cu cm for Fe-Ni-Mn and the most widely used previous estimate of n_i is 10^7 per cu cm.[4,6,13] Indeed, even if all the particles which transform at 195°K in Fe-Ni-Mn are counted, the effective nucleation site density in less than 10^6 per cu cm. Note also that $n^{*\prime}(Q)$ increases with decreasing temperature, Table IV, and thus with the larger driving forces applicable to some experiments $n^{*\prime}(Q)RT$ could be somewhat higher. Further, use of the present numbers from experiments on small solidified particles for estimation of the number of nucleation sites in bulk annealed specimens would obviously be a questionable procedure. Nonetheless, it appears that lower estimates (*e.g.*, 10^5 per cu cm) of n_i would be more reasonable in analysis of bulk isothermal kinetics.

Variation of Activation Energy with Temperature

Before discussing the variation in activation energy with temperature, it is worthy of note that alloys such as Fe-Ni-C have not generally been studied in previous isothermal experiments. This is because in the bulk they "burst" upon transforming, *i.e.*, large autocatalytic effects predominate and extensive transformation (as great as 0.7) occurs as the first detectable event.[20] In the small particle experiments, the kinetics of initiation of these events is open to study because the potent autocatalysis is controlled and different particles nucleate martensite at different times and temperatures. It is of some interest that many of the kinetic features of the two alloys are the same when viewed on this level. For example, the isothermal kinetics in both cases supports the previously advanced idea that bursting is a prime cause of the very different macroscopic kinetics in these alloys.[21]

The point which is most interesting, however, is the kinetic feature that differs most between the two alloys. Specifically, Fig. 13 shows that Q_{min} is much more dependent on temperature for Fe-Ni-C than for Fe-Ni-Mn. The derivative, dQ/dT, can be referred to as the "apparent" activation entropy and is $67R$ for the Fe-Ni-C alloy and $36R$ for Fe-Ni-Mn for straight lines through all the data.

The magnitude of these "apparent" activation entropies are too large to attribute solely to a true ac-

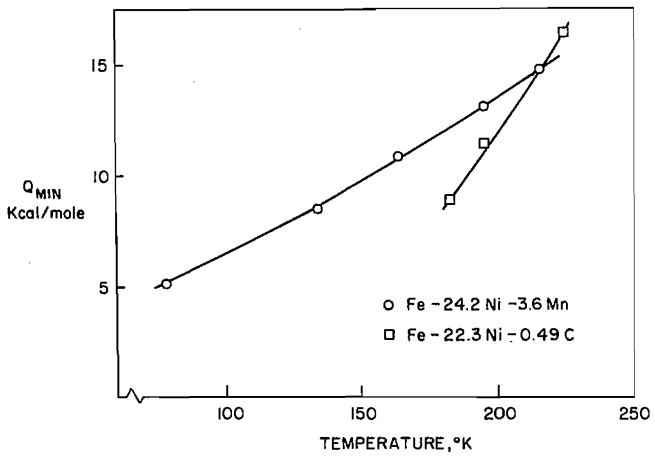

Fig. 13—The minimum observed activation energy (at $\nu = 10^{11}$ sec^{-1}) as a function of temperature for the two alloys.

tivation entropy[22] (particularly the Fe-Ni-C results). Instead, we note that the observed quantity (dQ/dt) contains at least two distinguishable effects; thus,

$$b \equiv \frac{dQ}{dt} = \frac{\partial Q}{\partial T} + \frac{\partial Q}{\partial \Delta G_v} \frac{\partial \Delta G_v}{\partial T} \quad [17]$$

or

$$b = S^a + V_{\Delta G} \Delta S_v^{\gamma-\alpha'} \quad [18]$$

where S^a is the activation entropy, $V_{\Delta G}$ can be referred to as an activation volume, and $\Delta S_v^{\gamma-\alpha'}$ is the chemical entropy change associated with the austenite-martensite phase change. Since appreciable activation entropies are unlikely, explanations of the difference in apparent activation entropy for the two alloys must be based on differences in the dependence of Q on ΔG_v. In the Kaufman-Cohen model,[5] the difference then could be rationalized by differences in either the "size" (potency) or surface energy of the embryos in the two alloys.

For a model that associates the critical nucleation step with the activation of dislocation motion, it has previously been pointed out[2] that the dependence of activation energy on driving force can be related to an activation volume for the critical dislocation motion. The driving force gives rise to a shear stress acting on the dislocations and this reduces the activation energy. Thus, changes in driving force will lead to changes in activation energy with the magnitude given by

$$\frac{\partial Q}{\partial \Delta G_v} = \frac{\partial Q}{\partial \tau} \frac{\partial \tau}{\partial \Delta G_v} \quad [19]$$

where $\partial Q/\partial \tau \equiv V_d$ is the activation volume for the deformation step. We can calculate V_d from the apparent activation entropies using Eqs. [18] and [19] and assuming $S^a = 0$, $\partial \tau/\partial \Delta G_v = 5.0$ (the reciprocal of the observed macroscopic shear), and $\Delta S_v^{\gamma-\alpha'} = 1$ cal per mole°C;[23] the results are

$$\begin{aligned} V_d &= 14.3\,\Omega \text{ (Fe-24 Ni-3.64 Mn)} \\ V_d &= 26.8\,\Omega \text{ (Fe-22 Ni-0.48 C)} \end{aligned} \quad [20]$$

where Ω is the atomic volume. Both of these numbers are in the range of activation volumes obtained from deformation experiments on similar fcc and bcc alloys.[24,25] They are also consistent with several possible specific mechanisms. The larger activation volume for Fe-Ni-C is indicative of a mechanism involving (relatively) longer-range interactions.

This magnitude of difference could arise from the critical step involving motion of different kinds of dislocations in the two cases or from a difference in the barrier at the critical step.* The difference in activation volume is not exceedingly large particularly since the differing martensite morphologies indicate that different lattice invariant shears occur in the formation of martensite in the two alloys. Indeed, it has been recently suggested that the difference in morphology can be attributed to the two alloys having different ways of minimizing the *plastic* work involved in forming martensite.[26,27] However, not enough is known about the details of the deformation mechanisms at the macroscopic stage—let alone whether the same mechanisms are of concern at the critical or nucleation stage—to allow one to see if these ideas have any furthur quantitative validity. In particular, would the expected deformation mechanisms for the two cases yield activation volumes in the order calculated above for the two alloys? This question provides fertile ground for theoretical work since the results show that these differences in activation volume lead to marked differences in the kinetic behavior.

*The martensite in the Fe-Ni-C alloy probably nucleates near the surface and this mechanism could differ. However, bulk results on Fe-Ni alloys[4] suggest that morphology is more important.

Implications of a Distribution

The result that the nucleation process is not singly activated does not prove that there are different basic nucleation mechanisms. Indeed, for a heterogeneous process, details about the surrounding of the site should lead to different extraneous forces and thus even for a given process could lead to a variety of activation energies. Therefore, although the issue of a distribution of effectiveness has often been ignored for martensite nucleation, it is consistent with heterogeneous processes. It would appear that nucleation theories will have to be capable of accounting for the distribution and ideally might predict the shape of the distribution curve. A preliminary start can be made in this direction by noting that the activation energy can be decreased by local stresses (in the manner of Eq. [19]). Thus the distribution of the strain energy density in a crystal containing dislocations could be used to rationalize distributions such as seen in Fig. 12(*a*). There would be a maximum strain energy density around the dislocation cores (corresponding to Q_{min}) and certain arrangements of dislocations could yield equal probability of finding regions with lower strain energy densities (other higher Q's).

At this point, it is useful to note that the dependence of $n^{*\prime}(Q)$ on temperature, Table IV, has also not been explained. It can be rationalized by hypothesizing that the activation volume, V_d, increases as the activation energy increases. This behavior would also be consistent with results from deformation studies.[24]

The concept of a distribution of nucleation site effectiveness suggests several questions whose answers might help clarify the nature of the nucleation site. For example, is Q_{min} and/or $n^{*\prime}(Q)$ affected by prestrain? Any of these possibilities can lead to increases in rate often found.[28] The same question can be viewed regarding autocatalysis; at present[6] it is assumed that Q_{min} is unchanged while $n^{*\prime}(Q)$ is increased. Results from experiments where the entire distribution is studied in the manner developed here might thus bring further light on the nature of the sites and the martensite nucleation mechanism.

SUMMARY

The present technique allows measurements of reaction rate due solely to the sites present initially and this makes it possible: 1) to determine that there is no nucleation time, 2) to show that a simple number of nucleation sites is an oversimplified concept in that the sites have a distribution of effectiveness and 3) to determine the isothermal kinetics of martensite formation in an Fe-22 Ni-0.49 C alloy.

The activation energy for nucleation and its dependence on temperature are derived from the present work with one less arbitrary parameter (the number of nucleation sites). The magnitudes of these quantities are not significantly different from previous estimates. Further, the apparent activation entropy differs for the two alloys and it is suggested that this indicates differing deformation mechanisms at the nucleation stage for martensite in the two alloys.

ACKNOWLEDGMENTS

The author is grateful to Drs. N. A. Gjostein and K. R. Kinsman for helpful critical reviews of the manuscript. During the course of the work, helpful discussions were held with Drs. K. R. Kinsman, G. R. Kotler, A. D. Murray, and P. Wynblatt. The author is particularly grateful for the painstaking technical assistance of J. P. Ingall.

REFERENCES

1. C. H. Shih, B. L. Averbach, and M. Cohen: *AIME Trans.*, 1955, vol. 203, pp. 183-87.
2. C. L. Magee: *Phase Transformations*, pp. 115-56, ASM, 1970.
3. D. G. McMurtrie and C. L. Magee: *Met. Trans.*, 1970, vol. 1, pp. 3185-91.
4. V. Raghavan and M. Cohen: *Met. Trans.*, 1971, vol. 2, pp.
5. L. Kaufman and M. Cohen: *Progr. Metal Phys.*, 1958, vol. 7, pp. 165-246.
6. V. Raghavan and A. R. Entwisle: Iron and Steel Inst., Spec. Rept. No. 93, 1965, pp. 30-37.
7. R. E. Cech and D. Turnbull: *AIME Trans.*, 1956, vol. 206, pp. 124-32.
8. D. Turnbull: *Impurities and Imperfections*, pp. 121-44, ASM, 1955.
9. D. Turnbull: *J. Chem. Phys.*, 1952, vol. 20, pp. 411-24.
10. R. E. Cech and J. H. Hollomon: *AIME Trans.*, 1953, vol. 197, pp. 685-89.
11. G. V. Kurdjumov and O. P. Maxsimova: *Dokl. Akad. Nauk. SSSR*, 1951, vol. 81, pp. 565-69.
12. R. L. Fullman: *AIME Trans.*, 1953, vol. 197, pp. 447-52.
13. S. R. Pati and M. Cohen: *Acta Met.*, 1969, vol. 17, pp. 189-99.
14. A. S. Nowick and B. S. Berry: *IBM J. Res. Dev.*, 1961, vol. 5, pp. 297-320.
15. A. V. Tobolsky: *Properties and Structures of Polymers*, pp. 117-35, J. Wiley and Sons, Inc., 1960.
16. R. M. Kimmel and D. R. Uhlmann: *J. Appl. Phys.*, 1969, vol. 40, pp. 4254-60.
17. W. Primak, *Phys. Rev.*, 1955, vol. 100, p. 1677-89.
18. W. Primak, *J. Appl. Phys.*, 1960, vol. 31, pp. 1524-33.
19. H. F. Weinberger, *Partial Differential Equations*, p. 347, Blaisdell Publ. Co., 1965.
20. J. C. Bokros and E. R. Parker: *Acta Met.*, 1963, vol. 11, pp. 1291-1301.
21. C. L. Magee: Ph.D. Thesis, Carnegie Institute of Technology, 1966.
22. K. C. Russell: *Met. Trans.*, 1971, vol. 2, pp. 5-12.
23. K. R. Satyanarayan, W. Eliasz, and A. P. Miodownik: *Acta Met.*, 1968, vol. 16, pp. 877-87.
24. P. Wynblatt and J. E. Dorn: *Trans. TMS-AIME*, vol. 236, pp. 1451-56.
25. G. F. Bolling and R. H. Richman: *Phil. Mag.*, 1969, vol. 19, pp. 247-64.
26. R. G. Davies and C. L. Magee: *Met. Trans.*, 1970, vol. 1, pp. 2927-31.
27. R. G. Davies and C. L. Magee: *Met. Trans.*, 1971, vol. 2, pp. 1939-47.
28. J. F. Breedis: *Acta Met.*, 1965, vol. 13, pp. 239-50.